

Zinc Ferrite/Polyaniline Composite Particles: Pigment Applicable as Electro-Active Paint

Lenka Munteanu¹, Andrei Munteanu¹ **Chyba! Záložka není definována.**, Michal Sedlacik^{1,2*}, Erika Kutalkova¹ **Chyba! Záložka není definována.**, Miroslav Kohl³, Andrea Kalendova³

¹ Centre of Polymer Systems, University Institute, Tomas Bata University in Zlín, Trida T. Bati 5678, 760 01 Zlín, Czech Republic

² Department of Production Engineering, Faculty of Technology, Tomas Bata University in Zlín, Vavreckova 275, 760 01 Zlín, Czech Republic

³ Faculty of Chemical Technology, University of Pardubice, Studentská 573, CZ-532 10 Pardubice, Czech Republic

* Corresponding author: msedlacik@utb.cz (M. Sedlacik)

Abstract

Hybrid conductive paint pigments composed of zinc ferrites (ZF) and polyaniline (PANI) were analysed as both a potential electro-active and corrosion-protective paint from the electrorheological (ER) point of view. The particles were characterised using scanning electron microscopy and X-ray diffraction spectroscopy. These hybrid conductive particles are used as pigments suitable for applications in paints which was confirmed by determining the consumption of linseed oil, the specific conductivity of aqueous extracts and the density of the tested pigments according to the relevant standardized methods. The chemical stability of particles was evaluated by means of durability tests in aggressive environment showing excellent results for the coated particles. Both ZF/PANI particles and pure ZF were dispersed in silicone oil and their ER behaviour was analysed through controlled shear rate and dynamic oscillatory tests. The ER performance of the pure ZF and the composite ZF/PANI suspensions were compared, showing promising results and enhanced ER performance of the later. Lastly,

the results were further validated via dielectric spectroscopy. Thus, the ZF/PANI particles have the potential to be applied as a hybrid ER fluid and an electro-active paint.

Keywords: electrorheology; zinc ferrite; anti-corrosive paint; electro-active paint; benzoic acid dopant; conductive polymer

1 Introduction

Zinc-rich paints have been in the spotlight in several forms, as the conductive property of zinc particles provides additional cathodic protection, thus prolonging the inhibition of corrosion process in an aggressive environment [1]. Subsequently, zinc has been widely used as a protective coating for decades [2], starting with the success of zinc-chromate followed by zinc-phosphate. However, the chromate modification was eventually discovered to be toxic and the phosphate variation, although showing satisfying results, has not surpassed the chromium protection performance [3]. According to certain studies, zinc ferrites (ZF) seem to offer a satisfying alternative [4,5], especially in a nano-sized form [6,7]. Other studies include a combination of ZF and conductive polymers which also present an attractive direction for further studies. These polymers have gained considerable attention in many fields and corrosion protection is no exception [8-11]. Olad and Hasouli [12] confirmed that composites combining polyaniline (PANI) and ZF featured an improved anti-corrosion performance in comparison with the pure PANI. Additionally, zinc is still classified as harmful to aquatic environment, although it is not generally as toxic as its chromate modification. This leads to another advantage of the polymer inclusion: partial substitution and therefore reduction of zinc amount without compromising the corrosion protection efficiency [13]. Also, it should be noted that PANI can be synthesised in multiple colour modification [14].

Corrosion protection plays a significant role in a distinct field – electrorheology, as it prolongs the lifetime of application devices [15]. An electrorheological fluid (ERF) is a smart system whose flow properties rapidly change upon exposure to an external electrical field. The ERF is composed of conductive particles, the so-called dispersed phase, dispersed in a non-conductive liquid carrier. The dispersed phase responds to the electric field by forming chain-like structures across the electrode gap enhancing the shear stress and other key properties. Thus, it enables a reversible fluid to solid-like state transformation in a matter of milliseconds (ER effect). This

effect is dependent on a number of parameters, for instance, the dielectric properties, particle size, morphology and conductivity, as well as particle concentration [16].

Despite the numerous ERF studies of conductive polymers [17], PANI in particular has been in the limelight due to its wide versatility. The success story of the PANI usage is mainly based on its thermal and environmental stability, easy synthesis and processability, and low cost [18]. Furthermore, it is available in multiple morphology forms [19] and its controllable conductivity is often achieved through protonation [20] or doping/de-doping process [21]. Modifying the specific conductivity of PANI by doping using protonation is interesting because an inorganic or organic acid can help increase its specific conductivity by up to eight or ten orders of magnitude [50]. Santos et al. [22] confirmed that the degree of dopant acidity affects the degree of PANI conductivity. In addition, Kohl et al. [23-25] investigated the influence of various PANI dopants used in protective paints on the corrosion inhibition performance.

Polyaniline, however, still possesses certain drawbacks regarding ER applications as it achieves rather low yield stress, colloidal instability, and its extraordinary conductivity leads to high current density unless it is properly controlled [26]. One way of overcoming these shortcomings while keeping its benefits is combining PANI with other particles in the form of core-shell structures. A broad range of studies has been focused on the composite particle variety [27,28], including hybrid composites combining organic and inorganic particles. In general, such composites give an access to advantageous properties of both parts while covering individual weaknesses [29].

In addition, ferrites with numerous modifications have been researched as potential smart materials in the ER field, and more frequently as a magnetorheological (MR) material [30-32]. Most of the research has been focused on modified ferrites or the above-mentioned core-shell based dispersions. Some sources reported modified ZF suspensions exhibiting dual ER and MR

response in a form of ZF/PANI microspheres [33] or Pickering emulsion [34] and similarly, ZF have been reported in combination with other conductive polymers [35,36].

This study aims to explore the properties of the hybrid core-shell ZF/PANI particles from electro-activity point of view. To our knowledge, this is the first hybrid material potentially studied for its application as ERF and protective anti-corrosion paint. Furthermore, the rheological properties of the pure and PANI-coated ZF dispersions are compared. Benzoic acid as PANI dopant is of a particular importance, as it was analysed for its anti-corrosive properties in past [37-39], but has not been covered in terms of electrorheology, so far.

Thus, as stated above, ferrites, especially zinc ferrites (ZFs), are being investigated for applications in anti-corrosion coatings [40]. They show a certain specific electrical conductivity, which is advantageous for the application of their chemical and electrochemical mechanism of protective action in paint binders. Increasing the specific electrical conductivity of these pigments using salts of conductive polymers in many cases also brings an increase in the resulting anti-corrosion effect in polymer coatings [55]. The resulting protective effect depends not only on the chemical composition, morphology, surface properties and structure of the pigment particles, but also on the type of conductive polymer applied, its protonation method, preparation technology and a number of other factors [56, 57]. The expected synergistic effect, or the positive influence of the conductive polymer on the pigment particles, is appropriate for the given purposes to be verified experimentally and to compare/quantify the properties of both forms. Therefore, in this study, hybrid zinc ferrite particles (ZF/PANI-B and ZF/PANI-P) with surface treatment with conductive polymers and particles without conductive polymers (ZF) were investigated in this study.

2 Experimental

2.1 Materials

2.1.1 Characterization of the starting materials

Two types of particles were used. First the red hematite α -Fe₂O₃ (manufacturer Lanxcess AG, Germany), which includes a synthetic hematite structure and regular nodular-shaped particles. Other properties include density: 5.1 g cm⁻³; colour: red; relative molecular weight (M_r): 159.69 g mol⁻¹; and lastly, the mean particle size (particle distribution median) is 0.546 μ m.

Silver grey lamellar α -Fe₂O₃ particles (manufacturer Lanxcess AG, Germany), labelled as specularite were chosen as the second material. The particle content is estimated to be 98% with clinochlore balance. The M_r is 159.69 g mol⁻¹ and particle distribution median is roughly 23.57 μ m.

Lastly, zinc oxide (ZnO) with a zincite structure was used as the final material for the pigment preparation, with density of 2.75 g cm⁻³ and M_r of 81.389 g mol⁻¹, imported by Lach-Ner s.r.o., Czech Republic.

2.1.2 Synthesis

Zinc ferrite pigments were synthesized by a high-temperature solid-phase process (calcination) of the above-mentioned starting material mixture, similarly to our previously utilized method [40]. Each synthesis procedure encompassed several steps, including homogenization of the starting materials mixture, calcination, rinsing, milling, and drying. The pigments were calcined at 1050 °C, the holdup time at the maximum temperature was 4 hours, the temperature ramp was 5 °C min⁻¹. Red hematite was selected as the starting source of Fe³⁺- cations for the synthesis of the first type ZF-type pigment. The aim of the synthesis using hematite as the starting material was to prepare pigments with primary particles possessing a generally isometric shape ZnFe₂O₄ (hematite). Similarly, specularite was chosen as the starting source of

Fe^{3+} - cations for the synthesis of second, this time lamellar, pigment type, in order to prepare primary lamellar-shaped ZnFe_2O_4 (specularite) pigment. Zinc oxide was selected as the sources of the divalent cations Zn^{2+} , in order to utilize its favourable contribution to the pigment's chemical anticorrosion behaviour.

The surface of both pure ZF pigment types - ZnFe_2O_4 (specularite) (ZF-S) and ZnFe_2O_4 (hematite) (ZF-H), was then covered with a layer of polyaniline-phosphate ($\text{ZnFe}_2\text{O}_4/\text{PANI-H}_3\text{PO}_4$ specularite and $\text{ZnFe}_2\text{O}_4/\text{PANI-H}_3\text{PO}_4$ hematite, respectively ZF/PANI-P-S and ZF/PANI-P-H) and a layer of polyaniline-benzoate ($\text{ZnFe}_2\text{O}_4/\text{PANI-C}_7\text{H}_6\text{O}_2$ specularite and $\text{ZnFe}_2\text{O}_4/\text{PANI-C}_7\text{H}_6\text{O}_2$ hematite, respectively ZF/PANI-B-S and ZF/PANI-B-H) during the polymerization of aniline in aqueous phosphoric or benzoic acid. As such, six types of pigments were synthesised. The overview of the pigments abbreviations is listed in Table 1.

Table 1: Code-naming

Name	Formula	Code-name
Zinc ferrite (specularite)	ZnFe_2O_4	ZF-S
Zinc ferrite (hematite)	ZnFe_2O_4	ZF-H
Zinc ferrite/polyaniline-phosphate (specularite)	$\text{ZnFe}_2\text{O}_4/\text{PANI-H}_3\text{PO}_4$	ZF/PANI-P-S
Zinc ferrite/polyaniline-phosphate (hematite)	$\text{ZnFe}_2\text{O}_4/\text{PANI-H}_3\text{PO}_4$	ZF/PANI-P-H
Zinc ferrite/polyaniline-benzoate (specularite)	$\text{ZnFe}_2\text{O}_4/\text{PANI-C}_7\text{H}_6\text{O}_2$	ZF/PANI-B-S
Zinc ferrite/polyaniline-benzoate (hematite)	$\text{ZnFe}_2\text{O}_4/\text{PANI-C}_7\text{H}_6\text{O}_2$	ZF/PANI-P-H

A colour change of the reacting ZF substance was apparent during the individual parts of the synthesis process. Initially, the mixture was transparent affected only by the presence of insoluble ZF powder pigment. Afterwards, it turned blue and finally, into green (typical for protonated emeraldine) as shown in Figure 1. As can be seen, Fig. 1 demonstrates ZF covered in PANI-P or PANI-B while presenting three stable forms of PANI and their transformations, including the colourless leucoemeraldine.

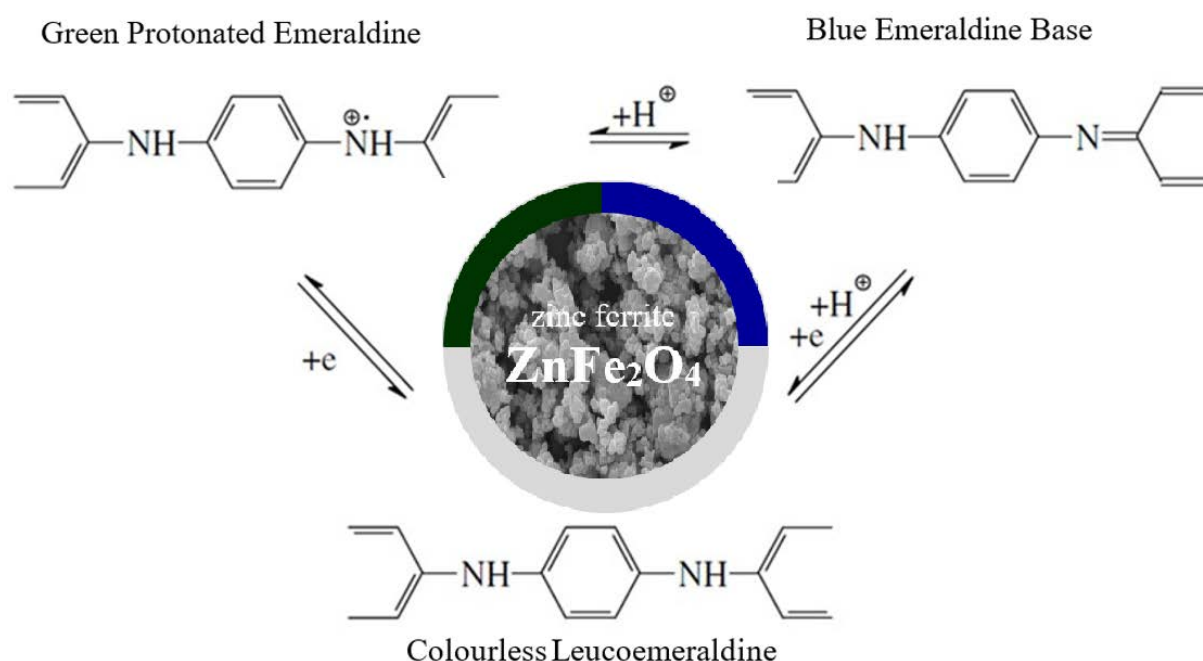


Figure 1: Stable forms of PANI and their conversions, schematic representation of the zinc ferrite particle covered with PANI phosphate/benzoate

2.1.3 Preparation of the pigments modified with a surface layer of polyaniline phosphate

The following process of both PANI-B and PANI-P modification of the pigments was inspired by our previously published research [41, 42]. The pigment $ZnFe_2O_4$ (21 g) was suspended in 250 mL of aniline (0.2 M) solution in 0.8 M ortho-phosphoric acid, and 250 mL of ammonium peroxydisulfate (0.25 M) also in 0.8 M ortho-phosphoric acid was added to initiate the aniline polymerization process at room temperature. The suspension was stirred for one hour during which aniline polymerized on the surface of the pigment particles. Next, the synthesised PANI-P was filtered out and rinsed with 0.4 M phosphoric acid, followed by acetone. The pigment

particles coated with the PANI-P overlayer were dried in air and then at 105 °C in a laboratory drier. The composite particles (ZF/PANI-P) contained about 30 wt.% polyaniline phosphate.

2.1.4 Preparation of the pigments modified with a surface layer of polyaniline benzoate

The second acid used to prepare the protonated form of PANI was benzoic acid. The PANI-B coating proceeded in the steps as the above mentioned ZF/PANI-P preparation. The layer modification procedure was the same, with the exception of 0.8 M solution of benzoic acid was used for the polymerization process. Afterwards, the suspension was stirred for one hour while aniline polymerized on the particle's surface. As above-described, filtering of PANI-B followed by rinsing with 0.4 M benzoic acid, as well as acetone. The PANI-coated particles were dried in the same procedure as their phosphate counterpart. The resulting ZF/PANI-B composite particles also contained about 30 wt.% polyaniline benzoate.

2.2 Particles characterization

The morphology of the dried non-dispersed particles was studied using a scanning electron microscope – Phenom Pro (SEM, Phenom-World, the Netherlands) operating at 10 kV.

Structural purity of hybrid conductive paint pigments was evaluated and their X-ray diffraction spectra were measured on a D8 Advance Diffractometer (Bruker AXS).

The density, oil absorption, and conductivity of particles were determined according to the relevant standardized methods as indicators for the possibility of their application to paint binders. A helium AutoPycnometer 1340 (Micromeritics, USA) was used to determine the pigments' specific weight (density). Linseed oil consumption was measured by the pestle-mortar method. To determine the conductivity, the powders were compressed to the form of pellets (diameter of 13 mm, thickness of 1 mm) by using a laboratory hydraulic press (Trystom Olomouc, H-62, Olomouc, Czech Republic). The electrical conductivity measurements were

evaluated using a Keithley 6517B (Keithley, Austin, TX, USA) multimeter and the four-point Van der Pauw method.

2.3 Preparation of electrorheological fluid

Prior dispersion, the particles were dried under vacuum to eliminate the potential condensation. Right after, each sample was dispersed in silicone oil (Lukosiol M200, Lučební závody Kolín, Czech Republic) in 5% particle volume fraction. Before measurements, the resulted suspensions were well-agitated and sonicated, to remove possible agglomerates.

2.4 Electrorheology

The ER behaviour was studied using Bohlin Gemini rotational rheometer (Malvern Instruments, UK) with a plate–plate geometry (20 mm in diameter). The gap between plates was set to 0.5 mm. The samples were tested under the presence and absence of an external electric field which was ranging from 0 to 3 kV mm⁻¹ (on and off-state, respectively) at room temperature. The current was generated by a DC high-voltage source TREK 668B (TREK, USA). The ER behaviour was examined in terms of both steady shear and oscillatory tests. Each measurement during the on-state was preceded by 1 min of activated electrical field. Every measuring period upon finishing was followed by 1 min of constant shear rate of 10 s⁻¹ without the presence of the electrical field in order to disperse the particles. For the oscillatory mode, the linear viscoelastic regime (LVE) was determined using dynamic strain sweeps prior to any other test.

2.5 Dielectric properties

The dielectric properties of the prepared ERFs were measured using the impedance dielectric spectroscopy analyser Novocontrol Concept 50 (Novocontrol, Germany), in the frequency

range of 0.01 Hz to 10 MHz at room temperature. The data were fitted using the Havriliak–Negami (H–N) model [43]:

$$\varepsilon^* = \varepsilon'_{\infty} + \frac{(\varepsilon'_0 - \varepsilon'_{\infty})}{(1 + \omega t_{\text{rel}})^{\alpha} \beta} \quad (1)$$

where ε^* represents the complex permittivity. The ε'_0 and ε'_{∞} are defined as permittivity at zero and infinite frequencies, their difference is later referred to as the relaxation strength $\Delta\varepsilon'$. ω stands for angular frequency; t_{rel} is the relaxation time; and α and β are shape parameters describing the asymmetry of the dielectric function (both in the range of 0–1).

2.6 Anti-corrosion properties

Excellent physical characteristics and anti-corrosion properties, including resistance to electrolytes or atmosphere containing sulfur oxides, are influenced by both, ZF-core of the particles and PANI-P or PANI-B [42] coating. In addition, chemical resistance of the pigment is also important. As such, the resistance to acid corrosion was tested at room temperature.

Chemical stability was investigated in the acidic pH range. In the basic region, the measurement was not performed due to the instability of the active conductive form of PANI (protonated polyaniline emeraldine “salt”) by transitioning to a non-conductive polyaniline base [51, 52]. The particles were dispersed in a hydrochloric acid (HCl) solution of 0.05 mol L⁻¹. The pH-meter (Greisinger electronic, GPRT 1400, AN, Germany) was calibrated with two standard buffer solutions (pH 4.00 and 7.00). The samples’ pH values were recorded every 5 minutes. Between each recording, the samples were well-stirred to avoid coagulation from sedimentation.

3 Results and discussion

3.1 Particles characterization

The prepared particles were examined using SEM which is shown in Figure 2. The magnification was adjusted to highlight the surface details. As can be seen, distinct morphology of examined particles was confirmed. To be exact, the natural specularite-based ZF resembles lamellar structures (Fig. 2a), while the synthetic ZF-H are rather of nodular shape (Fig. 2b). Considerably smaller size distribution is also apparent for the latter. As presented in Figure 3c and 3d, both ZF/PANI-B composite samples displayed changes in the surface morphology resulting from the PANI-B coating.

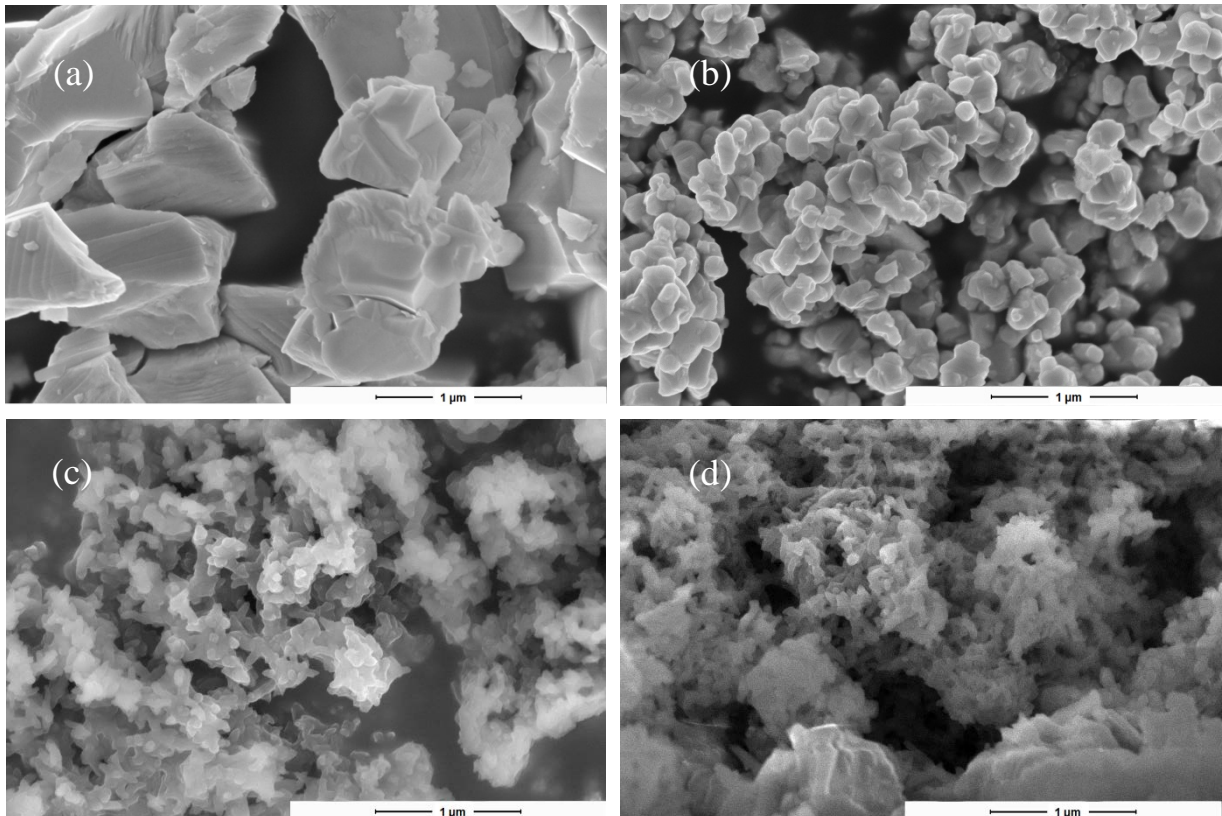


Figure 2: SEM images of ZF-S (a), ZF-H (b), ZF/PANI-B-S (c), and ZF/PANI-B-H (d).

X-ray diffraction analysis demonstrated that ZF-H and ZF-S with the normal spinel structure with the face-centred cubic lattice formed the homogeneous phase of the binary spinel (Fig 3a, Fig. 3b). P

The spectra (Fig. 3a, 3b) demonstrate that the reaction were completed and the appropriate structure were attained for both isometric ZF-H and non-isometric ferrite ZF-S [54]. Diffraction analysis of ZF-H coated with conductive polymers showed an X-ray amorphous content of conductive polymers of polyaniline-phosphate and polyaniline-benzoate (Fig. 3c, 3d).

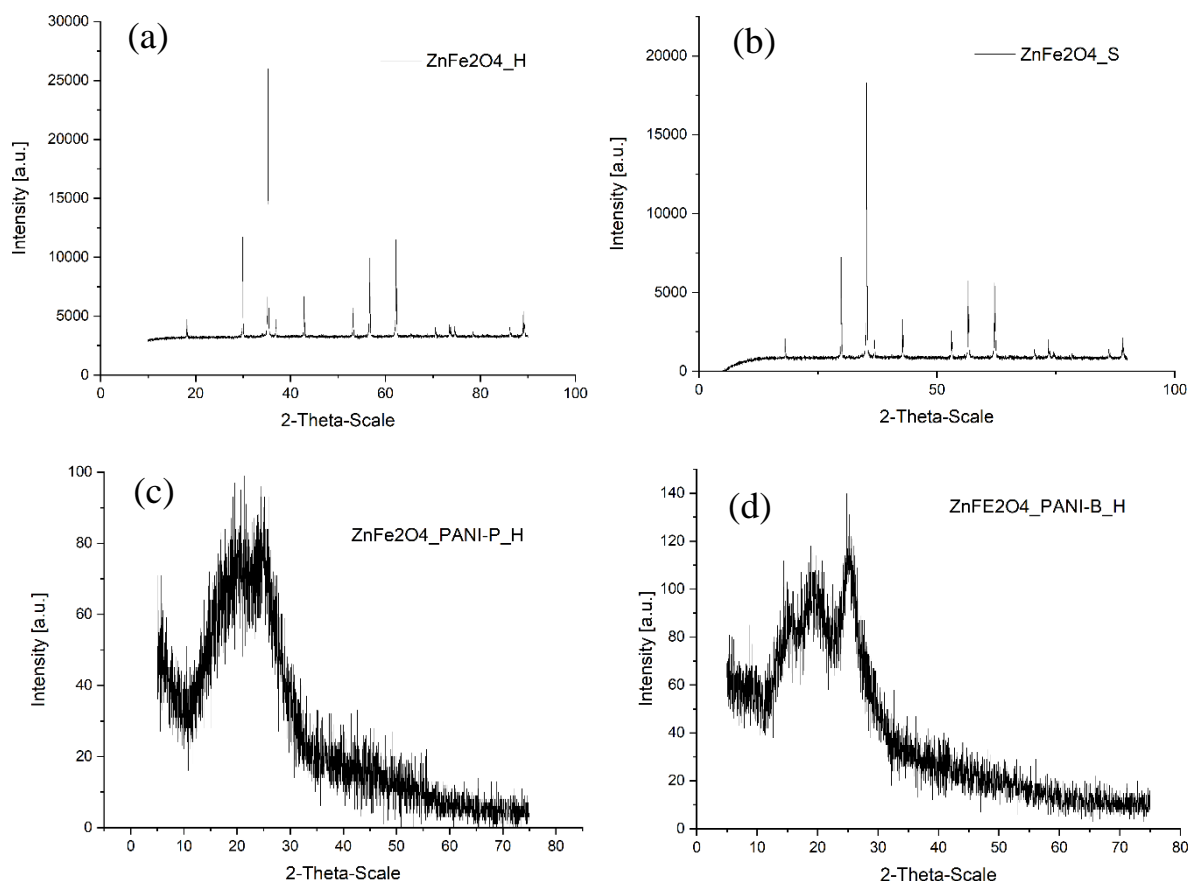


Figure 3: X. Results of X-ray diffraction analysis. Notes: (a) $ZnFe_2O_4$ (starting substance hematite. $\alpha-Fe_2O_3$); (b) $ZnFe_2O_4$ (starting substance specularite lam. $\alpha-Fe_2O_3$); (c) $ZnFe_2O_4/PANI-H_3PO_4$ (starting substance hematite. $\alpha-Fe_2O_3$); (d) $ZnFe_2O_4/PANI-C_7H_6O_2$ (starting substance hematite).

Furthermore, the prepared pigments were characterized by their basic characteristics in terms of so-called paint properties (Table 2). Density is one of the basic specific properties of powder materials and is an important indicator of their applicability in paints. The stability of the paint dispersion system depends, among other things, on the difference between the density of the pigment and the binder. Thus, the hybrid particles appear to be more advantageous for paint

applications. An important criterion in the production of pigmented paints is the smallest amount of binder needed to bind the pigment particles so as to form a cohesive pigment suspension in the binder. Therefore, the value of linseed oil consumption was determined for the tested pigments. Differences in the oil numbers of the individual pigments are caused not only by the different particle size, but also by the shape of the particles. The consumption of linseed oil in polyaniline-treated pigments was therefore higher than in uncoated pigments. Last but not least, conductivity was evaluated. As can be seen, the resulting conductivity of PANI shell differs with the type of dopant. This is in accordance with above-mentioned research results by Santos et al. [22]. It is important to note, that this study initially aimed to compare the effects of the benzoic acid and phosphate acid doping. However, the latter proved to be too conductive for ER measurements, causing short-circuit at low electric field. Therefore, the ZF/PANI-P were excluded from further measurement for the purposes of this article, nevertheless, they might be suitable for different applications (for instance, as purely corrosion-inhibiting paints [42]) in which the considerably higher conductivity would provide benefits.

Table 2: Pigment properties

Pigment	Density [g cm ⁻³]	Oil absorption [g/100 g]	Conductivity S m ⁻¹
ZnFe ₂ O ₄ (specularite)	5.12	13.05	1.61 × 10 ⁻¹⁰
ZnFe ₂ O ₄ (hematite)	5.46	13.15	1.88 × 10 ⁻⁶
ZnFe ₂ O ₄ /PANI-H ₃ PO ₄ (specularite)	2.65	58.33	2.44 × 10 ⁻³
ZnFe ₂ O ₄ /PANI-H ₃ PO ₄ (hematite)	2.57	56.36	6.18 × 10 ⁻³
ZnFe ₂ O ₄ /PANI-C ₇ H ₆ O ₂ (specularite)	2.59	72.00	2.69 × 10 ⁻¹⁰
ZnFe ₂ O ₄ /PANI-C ₇ H ₆ O ₂ (hematite)	2.58	70.00	2.16 × 10 ⁻⁹

3.2 Chemical stability

The behaviour of the dispersed particles in a corrosion-protection paint was previously demonstrated [25,40]. Presence of a PANI phosphate layer on the surface of ZF pigment particles resulted in an increased efficiency in the protection of the substrate metal against corrosion both in neutral environments and in acid environments. Both PANI phosphate on the surface of the zinc ferrite pigments and the pigments themselves have a passivating effect on the metal surface beneath the paint film [40]. The binder present of the coating material based on alkyd resin allowed conductive PANI phosphate to retain its electric charge, especially at the interface between the metal substrate and the coating film. This charge could be used to oxidize the underlying metal material to form a protective passive layer [40]. Following those conclusions, additional experiments evaluating the chemical stability of the particles were conducted.

Figure 4 reveals changes in pH of both pure and coated ZF particles dispersed in diluted HCl. As can be observed, the pure ZF particles manifested significant reaction with the acid as the pH value of the tested sample escalated especially during the first 20 min of the test, whereas the coated particles showcased constant pH value during the measurement. As demonstrated, the chemical stability of the coated particles in comparison to neat ZF was enhanced. This results from the benefit of the PANI-B shell, as PANI generally possess high chemical stability. As above-mentioned, this is also one of the reasons why PANI is in the spotlight of corrosion-protection paints. Generally, when corrosion affects the surface, PANI is able to release anions which function as local corrosion inhibitor. Although this process is irreversible and as such the protection may fade over time, it is also one of the reasons why PANI is in the spotlight as corrosion-protection coating [44].

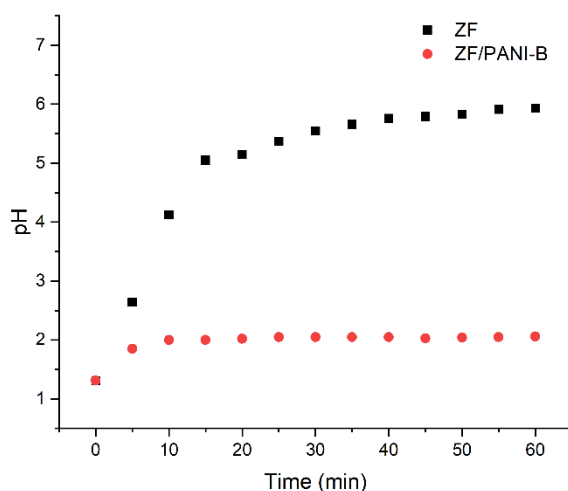


Figure 4: Chemical resistance of ZF and ZF/PANI-B particles against acidic environment of 0.05M HCl.

3.3 Electrorheology

To illustrate the changes given by the PANI-B shell, only the two most representative samples of the same base origin (hematite) and morphology are further compared for the ER performance evaluation. This also serves as a visual and clarity simplification of the later presented data.

The ER performance was firstly evaluated using a controlled shear rate (CSR) test while applying electric field through the sample in the range of 0–3 kV mm⁻¹. Figure 5 shows the changes of shear stress in the increasing shear rate in the range of 0.01–50 s⁻¹. As can be seen, at zero field, both samples exhibited a Newtonian behaviour. However, with the application of the electric field, the particles self-assemble into chain-like structures which results in a noticeable yield stress generation. The pure ZF displayed close to none changes in the electric field ranging between 1–3 kV mm⁻¹. In contrast, the coated ZF/PANI-B sample reached superior yield stress values compared to the former which can be attributed to the stronger chain-like formations of the coated particles. The Newtonian and Bingham plastic behaviours of the uncoated particles during the on and off-state are showed with the dash dot lines. When the electric field is applied the material obtains a yield stress at low shear rates. Eventually, the hydrodynamic forces overcome the electric with increase in shear rate and the material flows

in the same way as the off-state regardless of the magnitude of the electric field. From the Bingham model a critical shear rate can be found at $\sim 1 \text{ s}^{-1}$ where the hydrodynamic forces can be compared with the electric ones and the chain-like structure is starting to collapse as shown in the inserts of Fig. 5(a). For the coated particles on the other hand, the stable regime is extended to higher shear rates which cannot be captured in our experimental window. The extension of the yield stress regime by an order of magnitude is crucial in specific applications thus it is a desired enhancement of the fluids' ER properties [45].

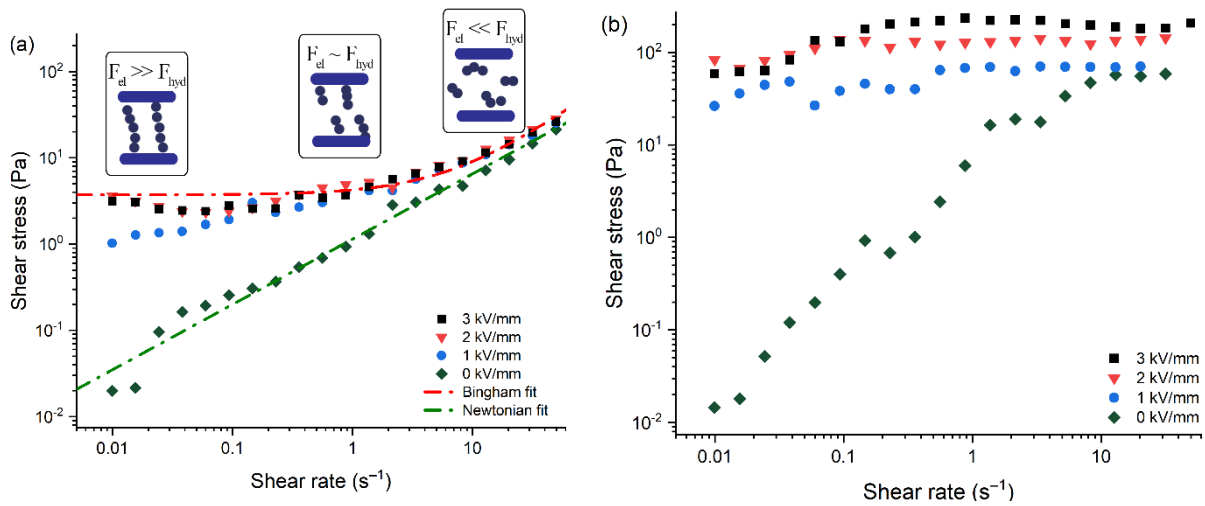


Figure 5: Flow curves for: pure ZF (a) and ZF/PANI-B (b). Dash dot lines correspond to the Bingham and Newtonian fits.

To demonstrate the reversibility of the ER performance of the individual samples, a step-wise test was performed (Fig. 6). The voltage was repeatedly switched on and off in interval of 30 s while the sample was sheared at 5 s^{-1} . The electric field was gradually increased each period (ranging from 0.5 to 4 kV mm^{-1}). As revealed in the Fig. 6, upon activating the electric field, the shear stress significantly rose immediately. Consequently, it dropped to its original value after the on-field period, proving the reversible nature of the ER effect. A noteworthy trend was demonstrated especially by the ZF/PANI-B curve as overall the shear stress grew to higher values proportionally to the increasing electric field. The uncoated counterpart showcased similar tendency, but the shear stress rise was rather minimal.

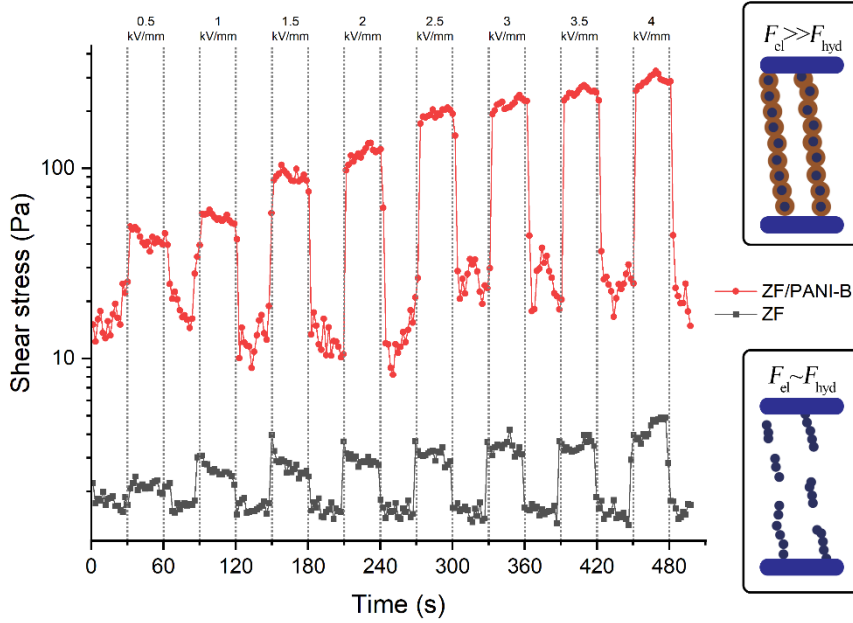


Figure 6: The effect of step-wise increase of electric field on shear stress at a shear rate of 5 s^{-1} . Changes of electric field activation are visualized by vertical dot lines and the particular electric field value.

To be exact, the majority of measured points in on-field from the 2 kV mm^{-1} interval onwards reached to shear stress of 2 to 3 Pa for the ZF sample. The only exception was the 4 kV mm^{-1} period, where it peaked over 4 Pa. On the other hand, the ZF/PANI-B exceeded 300 Pa in the final on-field period. Deducing from the results, the PANI-B shell considerably contributed to the enhancement of the ER performance of the ZF particles. Lastly, it is important to note that for the uncoated particles, the value of the shear rate corresponds to the region close the Newtonian regime where the chains should be almost collapsed in comparison with the coated particles for which the shear rate correspond to robust chains presence. The selected shear rate was chosen to demonstrate that the ER effect is still reversible in the intermediate regime where the electric forces are competing with their hydrodynamic analogues.

Finally, using the result data from CSR, the ER efficiency was calculated and presented in Fig. 7. This parameter is considered of great importance for evaluating ER materials [46]. The ER efficiency, according to Kutalkova [47], can be defined as:

$$e = \frac{\tau_e - \tau_0}{\tau_0} \times 100(\%) \text{ or } \frac{\eta_e - \eta_0}{\eta_0} \times 100(\%) \quad (2)$$

where τ_e and τ_0 stand for the values of shear stress in active and non-active electric field, respectively. Likewise, η_e and η_0 represent the viscosity in the same corresponding electric field status. The data acquired in the highest measured electric field strength (3 kV mm^{-1}) were applied as τ_e which was then converted to efficiency at different shear rates as shown in Fig. 5. As presented, the ZF/PANI-B achieved higher values in comparison to their uncoated counterpart. Thus, the significant enhancement of ER efficiency of the coated particles dispersion was confirmed.

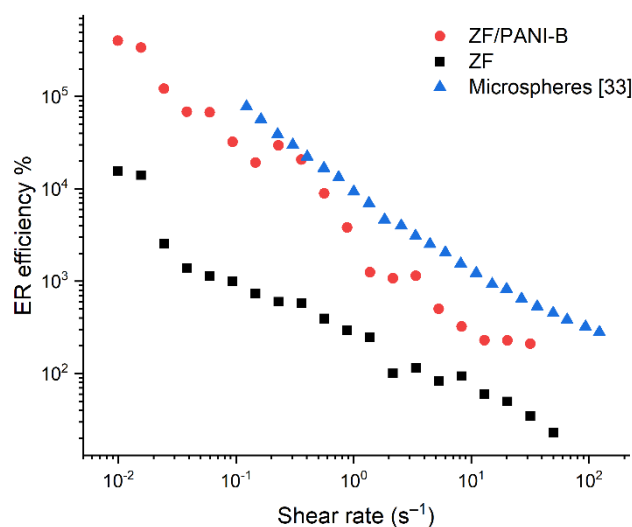


Figure 7: ER efficiency over increasing shear rate.

The data of ZF/PANI-B based ERF may be compared to a similar above-mentioned dual-performing ZF/PANI microspheres ERF, introduced by Kim et al. [33], in regards to the mutual ER performance. Firstly, taking the steady shear results into consideration, the results of ZF/PANI-B at 3 kV mm^{-1} reached higher values. However, in regards to ER efficiency, the ZF/PANI-B seem to have steeper decrease with the increasing shear rate, nevertheless, it should be considered as a minor difference. Overall, the compared ER performance seem to be a similar level for both, therefore it could be concluded, that the ER effect of ZF/PANI-B is at a satisfying level.

Moving to another ER analysis, the viscoelastic properties of the samples were measured using dynamic oscillatory tests. Prior to each frequency sweep test, an amplitude sweep measurement

was used as a pre-test to determine appropriate strain region fitting the LVE of the sample. Considering behaviour similarities of both measured ERFs, the shear strain of 0.004 % was set as it fits the LVE of both samples. The resulted data of storage G' and loss G'' moduli are presented in Fig. 8. As shown at zero field, both G' and G'' grew proportionally to the rising frequency with slopes close to 2 and 1, respectively, indicating the terminal flow-like behaviour. On the contrary, both G' and G'' showcased increased values in the activated electric field in form of a plateau. The plateau is proportionally increased with the values of the electric field strength similar to the abovementioned results.

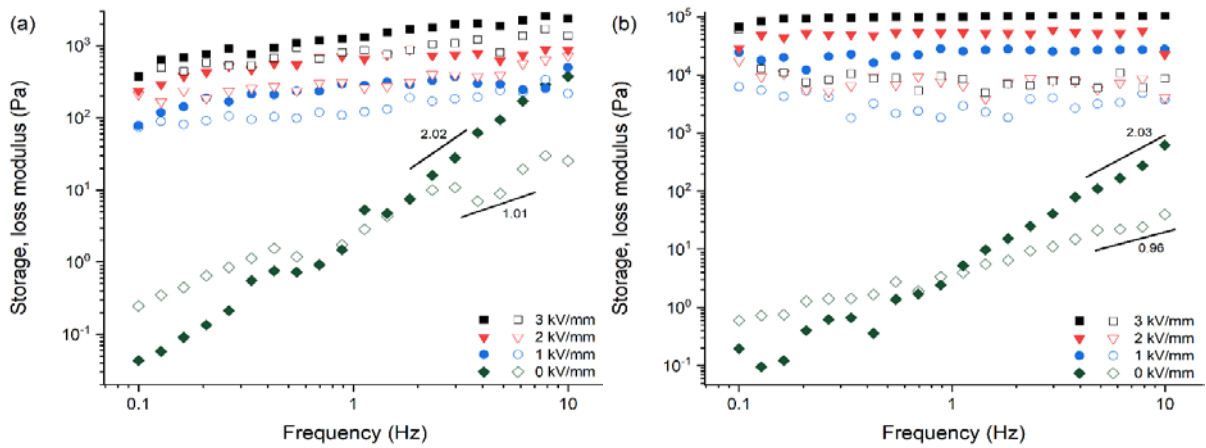


Figure 8: Storage (filled symbols) and loss moduli (open symbols) as a function of frequency under different electric field strengths: ZF (a) and ZF/PANI-B (b).

Additionally, the higher values of G' over G'' in on-state hints the domination of the elastic behaviour over the viscous one and a solid-like behaviour with the only exception in lower frequency in zero-field. This indicates that the substances became solid-like, when exposed to an electric field. This is a typical ER behaviour caused by chain-like formation of the dispersed particles in the direction of electric field [48,49]. Furthermore, comparing the pure ZF-based ERF with the core-shelled one during the on-state, a notable increment of two orders of magnitude for both moduli is observed for the latter. Therefore, the ZF/PANI-B sample proved to be a significant enhancement in this regard as well.

Figure 9 compares the storage modulus of coated and uncoated particles based on specularite and hematite during the on and off-state. Without the application of the electric field, both samples share an identical behaviour. During the on-state on the other hand, bare specularite-based particles show a higher plateau of G' thus better ER effect, which is likely caused by shape irregularity. In contrast, PANI-B coated hematite-based particles show a considerably higher increase of the plateau of G' in comparison to the specularite-based particles. It can be assumed that the smaller size of the former possesses larger active surface which leads to better interfacial polarization when particles are coated with conductive polymer (PANI-B in this case).

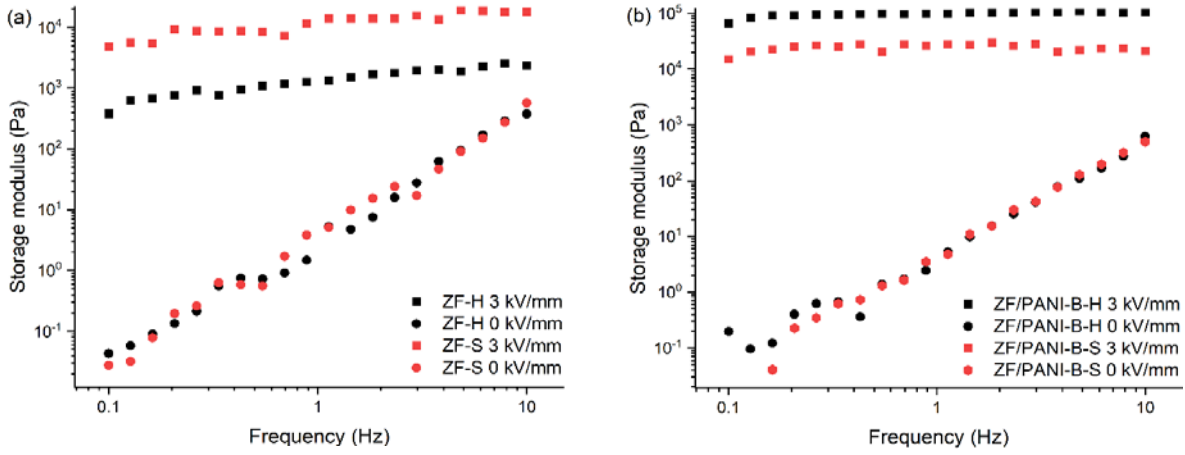


Figure 9: Storage modulus comparison of both hematite and specularite origins of ZF, uncoated particles (a), PANI-B coated particles (b).

3.4 Dielectric properties

The ER behaviour of the examined samples is generally known to be a result of interfacial polarization of the dispersed ER particles. Therefore, following the previous ER measurements, the dielectric spectroscopy was used to complement the data and to further compare the pure ZF and coated ZF/PANI-B samples. Figure 10 shows the data of permittivity values (ϵ' and ϵ'') as they were modelled and compared with the H–N model (Eq. (1)) to acquire the dielectric parameters. Consequently, the relaxation time τ_{rel} and dielectric relaxation strength $\Delta\epsilon$ were extracted into Table 3. As shown, the pure ZF-based ERF has a three orders of magnitude faster

relaxation time, however lower relaxation strength. This leads to a deduction that with the addition of PANI-B shell, the sample gained a higher ER potential given the increased dielectric strength, albeit, the polarization process became slower.

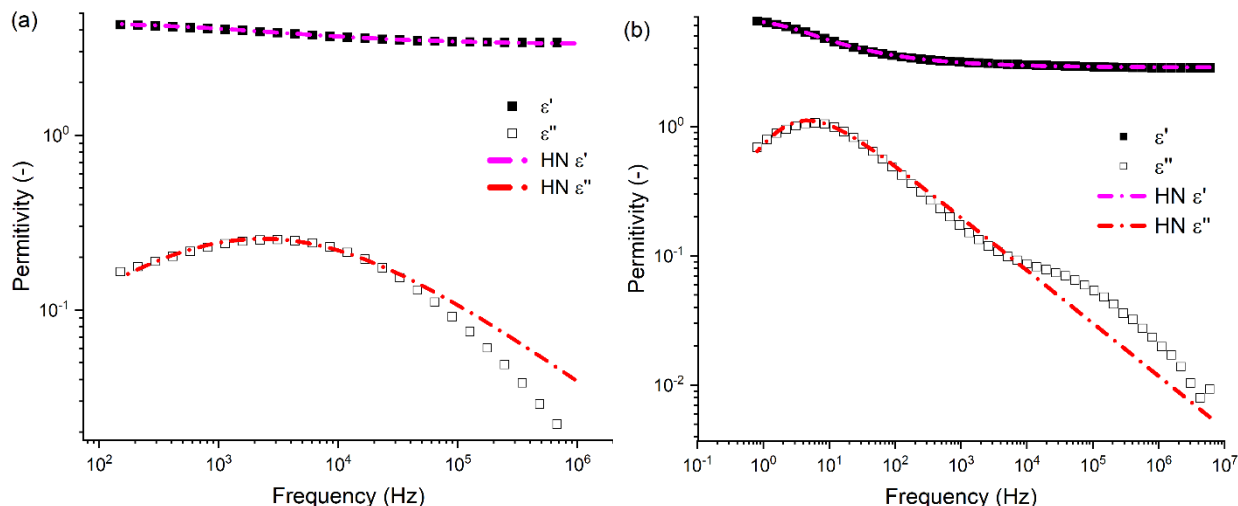


Figure 10: Dielectric spectra and H-N model curves: ZF (a) and ZF/PANI-B (b). The measured data are shown as squares while the H-N model fit is represented as dash dot lines.

Table 3: Dielectric properties of pure and core-shell dispersed ZF particles.

Particles	τ_{rel} [s]	$\Delta\epsilon$ [-]
ZF	0.0001	3.31
ZF/PANI-B	0.4482	4.01

4 Conclusions

The aim of this study was to complement the research of conductive ZF anti-corrosion pigments using two types of hematite (natural specularite and synthetic hematite) and PANI dopants and evaluate their potential as an electro-active paint base. This is the first recorded attempt to make a material functional as both ERF and protective anti-corrosion paint. Both particle types proved to be very similar in terms of ER behaviour while only one of the PANI dopants was able to enhance the materials as the phosphate acid proved to generate core-shell particles with too high conductivity for their application in ERFs.

Overall, the rheological tests have confirmed a satisfying ER response of ZF and ZF/PANI-B. The coated particles showed a much higher yield stress and the regime, in which the electric forces dominate of the hydrodynamic, was extended by at least an order of magnitude of the shear rate. Furthermore, the ERF proved to reversibly change its state both during the yield stress and close to Newtonian regime. During oscillatory tests the two different ores were compared with the hematite showing a better ER response for the coated particles. From the dielectric properties point of view, the pure ZF particles exhibited a shorter relaxation time, on the other hand, the coated particles featured a higher dielectric relaxation strength, which was considered as more important factor for ER performance in this study.

From the corrosion-protection perspective, the chosen ferrite spinel structure provides benefits resulting from its excellent properties. In addition, the cations in the oxide lattice can resolve the non-toxicity of the final compound. The mixed iron oxides and zinc ferrites with modified surface by a conductive polymer have the potential to extend the range of anticorrosion pigments and become integral components of systems for anticorrosion protection of metals as what is called smart coatings. The ferrite core also contributes to a better distribution of the conductive polymer through the paint film and increase the electrically conductive sites in the crosslinked polymeric paint film.

This study has addressed only the ER behaviour and it has not fully analysed sedimentation of the particles, which generally plays an important role in application of ERFs as well as in protective paints, nevertheless, it could offer an option for future in-detail research.

Since conductive ZF-based pigments are in the spotlight as corrosion-protection paints and proved their ER performance, this is the first assessment of these particles as such hybrid material applicable in both fields. As such, this may offer a unique opportunity to further pursue.

Acknowledgements

The authors gratefully acknowledge project DKRVO [RP/CPS/2022/007] supported by the Ministry of Education, Youth and Sports of the Czech Republic.

The authors also thank Dr. Robert Moučka, for his assistance with dielectric spectroscopy, and Dr. Milan Masař, for his assistance with scanning electron microscopy characterization.

Declaration of Competing Interest

The authors declare that they have no known competing financial interests or personal relationships that could have appeared to influence the work reported in this paper.

References

- [1] O.Ø Knudsen, U. Steinsmo, M. Bjordal, Zinc-rich primers—Test performance and electrochemical properties, *Progress in Organic Coatings*. 54 (2005) 224-229.
- [2] R.N. Jagtap, P.P. Patil, S.Z. Hassan, Effect of zinc oxide in combating corrosion in zinc-rich primer, *Progress in Organic Coatings*. 63 (2008) 389-394.
- [3] A.C. Bastos, M.G.S. Ferreira, A.M. Simões, Comparative electrochemical studies of zinc chromate and zinc phosphate as corrosion inhibitors for zinc, *Progress in Organic Coatings*. 52 (2005) 339-350.
- [4] A. Kalendová, Alkalisising and neutralising effects of anticorrosive pigments containing Zn, Mg, Ca, and Sr cations, *Progress in Organic Coatings*. 38 (2000) 199.
- [5] P. Benda, A. Kalendová, Anticorrosion Properties of Pigments based on Ferrite Coated Zinc Particles, *Physics Procedia*. 44 (2013) 185-194.
- [6] S. Mahvidi, M. Gharagozlou, M. Mahdavian, S. Naghibi, Potency of ZnFe₂O₄ Nanoparticles as Corrosion Inhibitor for Stainless Steel; the Pigment Extract Study, *Materials Research*. 20 (2017) 1492-1502.
- [7] A.U. Chaudhry, V. Mittal, M.I. Hashmi, B. Mishra, Evaluation of Ni_{0.5}Zn_{0.5}Fe₂O₄ nanoparticles as anti-corrosion pigment in organic coatings for carbon steel, *Anti-corrosion Methods and Materials*. 64 (2017) 644-653.
- [8] F. Assassi, N. Benharrats, Synthesis, characterizations and application of polyaniline-paint as anticorrosion agent, *Inorganic and Nano-metal Chemistry*. 51 (2021) 805-813.

- [9] N. Boshkova, N. Tabakova, G. Atanassova, N. Boshkov, Electrochemical Obtaining and Corrosion Behavior of Zinc-Polyaniline (Zn-PANI) Hybrid Coatings, *Coatings*. 9 (2019) 487.
- [10] M. Shabani-Nooshabadi, M. Mollahoseiny, Y. Jafari, Electropolymerized coatings of polyaniline on copper by using the galvanostatic method and their corrosion protection performance in HCl medium, *Surface and Interface Analysis*. 46 (2014) 472-479.
- [11] S. Ananda Kumar, K. Shree Meenakshi, T.S.N. Sankaranarayanan, S. Srikanth, Corrosion resistant behaviour of PANI–metal bilayer coatings, *Progress in Organic Coatings*. 62 (2008) 285-292.
- [12] A. Olad, H. Rasouli, Enhanced corrosion protective coating based on conducting polyaniline/zinc nanocomposite, *Journal of Applied Polymer Science*. 115 (2010) 2221-2227.
- [13] P. de Lima-Neto, A.P. de Araújo, W.S. Araújo, A.N. Correia, Study of the anticorrosive behaviour of epoxy binders containing non-toxic inorganic corrosion inhibitor pigments, *Progress in Organic Coatings*. 62 (2008) 344-350.
- [14] R.K. Yuan, Z.P. Gu, H. Yuan, Studies of controllable colour change properties of polyaniline film, *Synthetic Metals*. 69 (1995) 233-234.
- [15] H.J. Choi, M.S. Jhon, Electrorheology of polymers and nanocomposites, *Soft Matter*. 5 (2009) 1562-1567.
- [16] Y.Z. Dong, H.M. Kim, H.J. Choi, Conducting polymer-based electro-responsive smart suspensions, *Chemical Papers* 75 (2021) 5009-5034.
- [17] Q. Lu, W.J. Han, H.J. Choi, Smart and Functional Conducting Polymers: Application to Electrorheological Fluids, *Molecules*. 23 (2018) 2854.
- [18] J. Sebastian, J.M. Samuel, Recent advances in the applications of substituted polyanilines and their blends and composites, *Polymer Bulletin*. 77 (2019) 6641-6669.
- [19] M. Sedlacik, V. Pavlinek, M. Mrlik, Z. Morávková, M. Hajná, M. Trchová, J. Stejskal, Electrorheology of polyaniline, carbonized polyaniline, and their core–shell composites, *Materials Letters*. 101 (2013) 90-92.
- [20] J. Stejskal, J. Prokeš, M. Trchová, Reprotonation of polyaniline: A route to various conducting polymer materials, *Reactive & Functional polymers*. 68 (2008) 1355-1361.
- [21] T. Le, Y. Kim, H. Yoon, Electrical and Electrochemical Properties of Conducting Polymers, *Polymers*. 9 (2017) 150.
- [22] J. Santos, S. Goswami, N. Calero, M.T. Cidade, Electrorheological behaviour of suspensions in silicone oil of doped polyaniline nanostructures containing carbon nanoparticles, *Journal of Intelligent Material Systems and Structures*. 30 (2019) 755-763.
- [23] M. Kohl, A. Kalendová, Effect of polyaniline salts on the mechanical and corrosion properties of organic protective coatings, *Progress in Organic Coatings*. 86 (2015) 96-107.

- [24] M. Kohl, A. Kalendová, E. Schmidová, Enhancing corrosion resistance of zinc-filled protective coatings using conductive polymers, *Chemical Papers* 71 (2016) 409-421.
- [25] M. Kohl, A. Kalendová, P.P. Deshpande, E. Schmidová, Effects of conductive polymers (type and concentration) in coatings with zinc particles of different shapes, *Journal of Coatings Technology and Research*. 16 (2019) 949-962.
- [26] J.A. Marins, F. Giulieri, B.G. Soares, G. Bossis, Hybrid polyaniline-coated sepiolite nanofibers for electrorheological fluid applications, *Synthetic Metals*. 185-186 (2013) 9-16.
- [27] M.J. Kim, Y.D. Liu, H.J. Choi, Urchin-like polyaniline microspheres fabricated from self-assembly of polyaniline nanowires and their electro-responsive characteristics, *Chemical Engineering Journal*. 235 (2014) 186-190.
- [28] Y.Z. Dong, W.J. Han, H.J. Choi, Polyaniline Coated Core-Shell Typed Stimuli-Responsive Microspheres and Their Electrorheology, *Polymers*. 10 (2018) 299.
- [29] Y.D. Liu, H.J. Choi, Electrorheological response of polyaniline and its hybrids, *Chemical Papers*. 67 (2013) 849-859.
- [30] C.Y. Gao, E. Baek, C.Y. You, H.J. Choi, Magnetic-stimuli rheological response of soft-magnetic manganese ferrite nanoparticle suspension, *Colloid Polym Science*. 299 (2021) 865-872.
- [31] A.V. Anupama, V. Kumaran, B. Sahoo, Application of Ni-Zn ferrite powders with polydisperse spherical particles in magnetorheological fluids, *Powder Technology*. 338 (2018) 190-196.
- [32] G. Wang, Y. Ma, Y. Tong, X. Dong, M. Li, Solvothermal synthesis, characterization, and magnetorheological study of zinc ferrite nanocrystal clusters, *Journal of Intelligent Material Systems and Structures*. 28 (2017) 2331-2338.
- [33] H.M. Kim, S.H. Kang, H.J. Choi, Polyaniline coated ZnFe₂O₄ microsphere and its electrorheological and magnetorheological response, *Colloids and surfaces. A, Physicochemical and engineering aspects*. 626 (2021) 127079.
- [34] J.N. Kim, Y.Z. Dong, H.J. Choi, Pickering Emulsion Polymerized Polyaniline/Zinc-ferrite Composite Particles and Their Dual Electrorheological and Magnetorheological Responses, *ACS omega*. 5 (2020) 7675-7682.
- [35] S.H. Kang, H.J. Choi, Dynamic Response of Polyindole Coated Zinc Ferrite Particle Suspension under an Electric Field, *Materials*. 15 (2021).
- [36] T.H. Kim, H.J. Choi, Fabrication and Shear Response of Conducting Polymer-Coated Zinc Ferrite Particles Under Magnetic/Electric Field, *TMAG*. 58 (2022) 1-5.
- [37] C.A. Amarnath, S. Palaniappan, Polyaniline doped by a new class of dopants, benzoic acid and substituted benzoic acid: synthesis and characterization, *Polymers for Advanced Technologies*. 16 (2005) 420-424.

- [38] A.R. Elkais, M.M. Gvozdenović, B.Z. Jugović, B.N. Grgur, The influence of thin benzoate-doped polyaniline coatings on corrosion protection of mild steel in different environments, *Progress in Organic Coatings*. 76 (2013) 670-676.
- [39] B.N. Grgur, A.R. Elkais, M.M. Gvozdenović, S.Ž Drmanić, T.L. Trišović, B.Z. Jugović, Corrosion of mild steel with composite polyaniline coatings using different formulations, *Progress in Organic Coatings*. 79 (2015) 17-24.
- [40] J. Brodinová, J. Stejskal, A. Kalendová, Investigation of ferrites properties with polyaniline layer in anticorrosive coatings, *Journal of Physics and Chemistry of Solids*. 68 (5-6) (2007) 1091.
- [41] M. Kohl, A. Kalendová, J. Stejskal, The effect of polyaniline phosphate on mechanical and corrosive properties of protective organic coatings containing high amounts of zinc metal particles, *Progress in Organic Coatings*. 77 (2014) 512-517.
- [42] A. Kalendová, D. Veselý, M.Kohl, J. Stejskal, Anticorrosion efficiency of zinc-filled epoxy coatings containing conducting polymers and pigments, *Progress in Organic Coatings*. 78 (2015) 1.
- [43] S. Havriliak, S. Negami, A complex plane representation of dielectric and mechanical relaxation processes in some polymers, *Polymer*. 8 (1967) 161-210.
- [44] L. Zhang, W. Du, A. Nautiyal, Z. Liu, X. Zhang, Recent progress on nanostructured conducting polymers and composites: synthesis, application and future aspects, *Science China Materials*. 61 (2018) 303-352.
- [45] L. Linzhi, G. Shujuan, Polyaniline (PANI) and BaTiO₃ composite nanotube with high suspension performance in electrorheological fluid, *Materials Today Communications*. 24 (2020) 100993.
- [46] Y. Chen, W. Sun, H. Zheng, C. Li, B. Zhang, B. Wang, C. Hao, The electrorheological response behavior of small coral-like H₂Ti₂O₅@SiO₂ core-shell nanoparticles, *Journal of the Taiwan Institute of Chemical Engineers*. 129 (2021) 327-341.
- [47] E. Kutalkova, T. Plachy, J. Osicka, M. Cvek, M. Mrlik, M. Sedlacik, Electrorheological behavior of iron(ii) oxalate micro-rods, *RSC advances*. 8 (2018) 24773-24779.
- [48] C.S. Jun, S.H. Kwon, H.J. Choi, Y. Seo, Polymeric Nanoparticle-Coated Pickering Emulsion-Synthesized Conducting Polyaniline Hybrid Particles and Their Electrorheological Study, *ACS Applied Materials & Interfaces*. 9 (2017) 44811.
- [49] E. Kutalkova, A. Ronzova, J. Osicka, D. Skoda, M. Sedlacik, The influence of synthesis conditions on the electrorheological performance of iron(II) oxalate rod-like particles, *Journal of Industrial and Engineering Chemistry*. 100 (2021) 280-287.
- [50] J. Prokeš, J. Stejskal, M. Omastová, Polyanilin a polypyrrol dva představitelé vodivých polymerů, *Chemické listy*. 95 (2001) 484-492.

- [51] A. Kalendová, I. Sapurina, J. Stejskal, D. Veselý, Anticorrosion properties of polyaniline-coated pigments in organic Coatings, *Corrosion Science*. 50(12) (2008)3549-3560.
- [53] A. Kalendová, D. Veselý, J. Stejskal, Organic coatings containing polyaniline and inorganic pigments as corrosion inhibitors, *Progress in Organic Coatings*. 62(1) (2008) 105-116.
- [54] A. Kalendová, P. Ryšánek, K. Nechvílová, Investigation of the anticorrosion efficiency of ferrites $Mg_{1-x}Zn_xFe_2O_4$ with different particle morphology and chemical composition in epoxy-ester resin-based Coatings, *Progress in Organic Coatings*. 86 (2015) 147-163.
- [55] A. Kalendová, M. Kohl, Mechanical and anticorrosion efficiency of organic coatings with polyaniline phosphate and polypyrrole phosphate modified pigments, *Ochrona przed korozja*. 63(9) (2020) 278-289
- [56] M. Kohl, A. Kalendová, E. Černošková, M. Bláha, J. Stejskal, M. Erben, Corrosion protection by organic coatings containing polyaniline salts prepared by oxidative polymerization, *Journal of Coatings Technology and Research*. 14(6) (2017) 1397-1410.
- [57] T. Hájková, A. Kalendová, M. Kohl, Anticorrosion and physical properties of organic coatings containing perovskites surface modified by polyaniline or polypyrrole phosphates, *Chemical papers*. 71(2) (2017) 439-448.